Integration of Electrolysis Systems into isolated microgrid systems at extreme cold climates

Nils Nemsow
Institute for Technical Physics (ITEP)
Karlsruhe Institute of Technology (KIT)
Karlsruhe, Germany
0000-0002-7630-9421

Kumaraguru Prabakar
National Renewable
Energy Laboratory (NREL)
Golden, CO, USA
0000-0002-2962-0743

Ben McGilton
National Renewable
Energy Laboratory (NREL)
Golden, CO, USA
0000-0001-9317-3346

Rebecca Meadows
National Renewable
Energy Laboratory (NREL)
Golden, CO, USA

Giovanni De Carne
Institute for Technical Physics (ITEP)
Karlsruhe Institute of Technology (KIT)
Karlsruhe, Germany
0000-0002-3700-2902

Abstract—**Isolated microgrid systems are generally used to power communities in remote locations where transmission line installations are cost prohibitive. These systems are usually powered by diesel generators, delivering expensive energy with high carbon emissions. However, most of these communities have special geographic access to renewable energy. These special conditions make it interesting to investigate the deployment of renewable energies and storage solutions. Within this scope, this paper analyses the integration of water electrolysis systems into off-grid communities, simulating the electrolyzer as well as the whole electrical grid in real time.**

Index Terms—**Hydrogen, electrolysis, grid integration, digital real-time simulation.**

I. INTRODUCTION

The State of Alaska in the USA has one of the highest adoption rates of microgrids in the world [1] with more than 200 remote, non-grid connected communities. [2] Many communities are looking to transition to renewable energy to both address high-cost fluctuations in fossil fuels and to reduce greenhouse gas emissions. [3] To successfully achieve a transition to renewables, long term energy storage is key to account for the variability in renewable energy resources. [4]

An example of a small off-grid community is Igiugig in Alaska. [5] With an average electrical load of 40 kW and a rare peak load around 100 kW, the community is supplied by its three diesel generators of 65 kW each. The price for fuel imported is volatile, and the community of Igiugig paid nearly $10 per gallon for its diesel imports in 2023. The leadership at Igiugig Village Council (IVC) has been investigating the adoption of renewable energies in order to mitigate or even eliminate their dependency on fuel imports. [6]

Igiugig is located on the south bank of the mouth of the Kvichak River and Lake Iliamna, providing good conditions for hydrokinetic power. Since 2014, the community has progressed from a hydrokinetic test site to multiple deployments [6] of river generator (RivGen) systems built by ORPC [7]. Furthermore, with dropping hardware prices, solar PV is becoming now cost effective in some areas of Alaska, where considerable yields can only be expected in the spring and summer seasons. In 2022, the community completed their Comprehensive Energy Plan [6] with the goal to reduce their diesel fuel usage for electricity by 50 % by 2030. As of 2019, almost 25,000 gallons of diesel fuel are used for electricity production per year, and slightly more for heating. [6] Several renewable energy scenarios are being investigated, mainly focusing on the deployment of PV and battery systems.

This paper discusses the integration of an electrolysis unit as a part of a possible hydrogen energy storage plant into the electrical and the thermal system of the community. While the Igiugig community is not currently pursuing a hydrogen based long-term energy solution, the intention of this work is to explore the integration aspects of such systems to better inform similar communities, the hydrogen and microgrid industries, and researchers in the space.

Digital real-time simulations allow the analysis of the interaction between the electrolyzer and the grid. The simulations are carried out using RTDS digital real-time simulation hardware and software. [8]

After an introduction and thorough analysis of the electrical grid situation in the Igiugig community, the modeling of PEM electrolyzer systems will be discussed. It is not only concentrated on the stack modeling itself, but also includes auxiliary components and covers electrical as well as chemical and thermal layer analysis. This approach allows the system's integration into its environment, providing crucial information about the interaction between current, voltage, pressure and

temperature parameters. Subsequently, operation strategies of hydrogen storage plants for resilient grid operation will be outlined.

II. BACKGROUND ON ISOLATED MICROGRID SYSTEM UNDER CONSIDERATION

The grid of the Igiugig community is an isolated microgrid system with no connection to other electrical power systems.

A. State of the art

The main component of Igiugig's electrical grid is the powerhouse containing three diesel generators with a power rating of 65 kW each. It features a heat recovery loop, which provides heat to the water filtration plant [5] in order to avoid the freezing of drinking water, as well as space heating for the post office, store, and some offices. [6] In close proximity to the powerhouse, a Battery Energy Storage System (BESS) was installed. It has a power rating of 125 kW at a capacity of 250 kWh and can be operated in grid-forming mode. [9] Located at the riverside, the marine energy production unit RivGen is an underwater hydrokinetic generator. It has a rated power output of 40 kW at a flow speed of 2.25 m/s or 80 kW at 3.5 m/s. [7]

The distribution grid is a three-phase system operating at a rated line voltage of 12.47 kV and a nominal frequency of 60 Hz. With its primarily radial topology, the powerhouse is at the top of the feeder system, together with the BESS. The distribution lines are underground cables, and there are nine coupling points, numbered SC1-SC9 with load transformers or interfaces for additional generation. [9] There are plans to install a 200 kW solar PV plant at the end of the feeder, at SC9.

The loads of Igiugig are mainly considered residential or building loads, there are a few machine loads in the water treatment plant. Refrigeration, digital services, lighting and entertainment constitute the majority of the electricity use, with the primary consumers being the internet service provider, the school, the clinic and the airport. During the summer season, the average load is between 30 and 40 kW and in the winter season, the average load is between 40 and 50 kW with peaks up to 70 kW every night. BESS maintenance and testing generates a few load peaks of 100 kW. [9]

B. Hydrogen storage plant integration

Due to geographic restrictions, the electrolysis plant will be planned for connection at the end of the feeder system, at SC9. The coupling point is on distribution voltage level of 12.47 kV, three-phase. A direct DC coupling to the planned PV plant will be possible, but is not considered in this study. A heat buffer storage can be implemented in the electrolysis facility to provide space heating for houses, replacing diesel heaters.

III. ELECTROLYSIS MODELING

To simulate the integration of the electrolysis unit into the power system of Igiugig, a system-level model of the

electrolyzer is designed. Besides the power consumption and hydrogen production, the heat output of the system will also be considered. Hydrogen compression and storage and fuel cell modeling is not covered in this paper.

A. Cell/Stack modeling

An electrolysis cell can be modeled as a series of passive elements and a voltage source. The parameters of these passive elements and the voltage source are dependent on the cell temperature, electrode pressure levels as well as the cell current density, making the electrical characteristics highly non-linear. The example in Figure 1 shows the equivalent circuit for a PEM electrolysis cell, displaying the open-circuit voltage as a voltage source and the three modeled overvoltages as resistors.

Electrolysis systems comprise multiple stacks operated in parallel, with each stack being a series of single cells. Modeling of whole systems necessitates an adaptation of the parameters for the passive elements and voltage sources into lumped values for the whole system.

A rectifier and a buck converter supply the low-voltage, high-current electrolyzer with energy from the three-phase AC grid. Usually, electrolysis cells are operated in current mode, meaning they can be modeled as current-controlled voltage sources. Controlling the current to a given reference value has the advantage of a steady hydrogen flow, since the hydrogen production rate is proportional to the cell current. To make models comparable, it has become a habit to use the current density as a reference, which is the cell current per active cell area and usually given in A/cm².

Following the modeling approach of Pukrushpan and Stefanopoulou [10] with its adaptions for RTDS digital real-time simulation [8], the input signal is the stack current and the output signal is the stack voltage, a sum of the open-circuit voltage and the overvoltages, multiplied by the number of cells in a stack, as shown in Eq. 1.

$$V_{elz} = n_{cells} \cdot V_{cell} = n_{cells} \cdot (V_{oc} + V_{act} + V_{conc} + V_{ohm}) \quad (1)$$

1) Open-circuit voltage V_{oc}: The open-circuit voltage, often referred to as Nernst voltage, is temperature- and pressure-dependent and can be seen as the minimum voltage to overcome for the electrolysis to happen. With Δg_f^0 being the change in Gibbs free energy, R being the universal gas constant and F the Faraday constant, Eq. 2 can be numerically simplified [8] to the term in 3, being dependent on the stack temperature as well as the partial pressures of hydrogen and oxygen.

$$V_{oc} = \frac{-\Delta g_f^0}{2F} + \frac{RT_{st}}{2F} \ln \frac{p_{H_2} p_{O_2}^{0.5}}{p_{H_2O}} \quad (2)$$

$$V_{oc} = 1.229 - 8.5 \cdot 10^{-4}(T_{st} - 298.15)$$
$$+ 4.3085 \cdot 10^{-5} \cdot T_{st} \left(\ln p_{H_2} + \frac{1}{2} \ln p_{O_2} \right) \quad (3)$$

2) Activation overvoltage V_{act}: The chemical interaction between molecules in both anode and cathode are responsible for the activation overvoltage, which is composed of a non-current dependent part V_0 and a current dependent part $V_a\left(1-e^{-10i}\right)$, with i being the cell current density, as displayed in Eq. 4. Numerical approximations for V_0 and V_a yield to the terms in Eq. 5 and 6. The partial pressures of hydrogen and oxygen, as well as the saturation pressure values can be calculated according to [11] and [12], thus they will not be further explained here.

$$V_{act} = V_0 + V_a\left(1 - e^{-10i}\right) \tag{4}$$

$$V_0 = 0.279 - 8.5 \cdot 10^{-4}(T_{st} - 298.15)$$
$$+ 4.3085 \cdot 10^{-5} \cdot T_{st}\left(\ln\frac{p_{ca} - p_{sat}}{1.01325}\right.$$
$$\left. + \frac{1}{2}\ln\frac{0.1173(p_{ca} - p_{sat})}{1.01325}\right) \tag{5}$$

$$V_a = 1.618 \cdot 10^{-5}(1000 - T_{st})\left(\frac{p_{O_2}}{0.1176} + p_{sat}\right)^2$$
$$+ (1.8 \cdot 10^{-4} \cdot T_{st} - 0.166)\left(\frac{p_{O_2}}{0.1176} + p_{sat}\right) \tag{6}$$
$$- 5.8 \cdot 10^{-4} \cdot T_{st} + 0.5736$$

3) Concentration overvoltage V_{conc}: Especially for higher current densities, the concentration of the reactants at the place of reaction will be reduced as the reaction speed is very high. This leads to the concentration overvoltage as shown in Eq. 7. Here, i_{max} is the critical current density, usually around 3 A/cm² and C_2 is a pressure- and temperature-dependent parameter. Both are determined empirically, the numerical approximation for C_2 is given in Eq. 8 and 9.

$$V_{conc} = i\left(C_2\frac{i}{i_{max}}\right)^2 \tag{7}$$

if $\left(\frac{p_{O_2}}{0.1176} + p_{sat}\right) < 2$ atm:

$$C_2 = (7.16 \cdot 10^{-4} \cdot T_{st} - 0.622)\left(\frac{p_{O_2}}{0.1176} + p_{sat}\right)$$
$$- 1.45 \cdot 10^{-3} \cdot T_{st} + 1.68 \tag{8}$$

if $\left(\frac{p_{O_2}}{0.1176} + p_{sat}\right) \geq 2$ atm:

$$C_2 = (8.66 \cdot 10^{-4} \cdot T_{st} - 0.068)\left(\frac{p_{O_2}}{0.1176} + p_{sat}\right)$$
$$- 1.6 \cdot 10^{-4} \cdot T_{st} + 0.54 \tag{9}$$

4) Ohmic overvoltage V_{ohm}: The transfer of hydrogen (H^+) ions through the membrane, from anode to cathode, comes with an electric resistance, largely dependent on temperature and humidity level. The constant t_{mem} denotes the thickness of the electrolytic membrane (in cm), and σ_{mem} is its conductivity, which can be approximated as shown in Eq. 11. The ohmic overvoltage as a product of the cell current density and the ratio of membrane thickness and conductivity can be calculated as in Eq. 10.

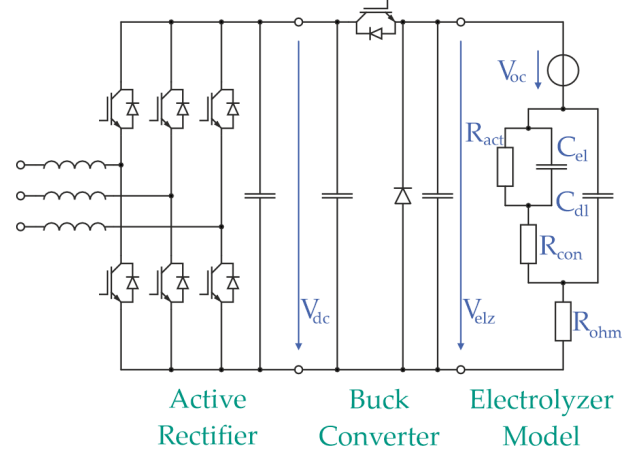$$V_{ohm} = R_{ohm} \cdot I = \frac{t_{mem}}{\sigma_{mem}} \cdot I \tag{10}$$

Fig. 1. Electrical system-level electrolysis model

$$\sigma_{mem} = (5.139 \cdot 10^{-3} \cdot \lambda_{mem} - 3.26 \cdot 10^{-3}) \cdot e^{350\left(\frac{1}{303} - \frac{1}{T_{st}}\right)} \tag{11}$$

The membrane humidity factor λ_{mem} represents the amount of water present in the electrolysis cell and its value ranges from 0 for a and entirely dry membrane to 15 for a fully hydrated membrane. If water is continuously supplied to the cell, the humidity factor can set to 15.

5) Polarization curve: The cell operating voltage V_{cell} against the current density i can be plotted for different temperature values, resulting in graphs as in Figure 2. The rated operation point is set to 1.2 A/cm² in this model. With a 111-cell stack and a cell area of 250 cm², this results in a rated stack current of 300 A at a rated stack voltage of 200 V.
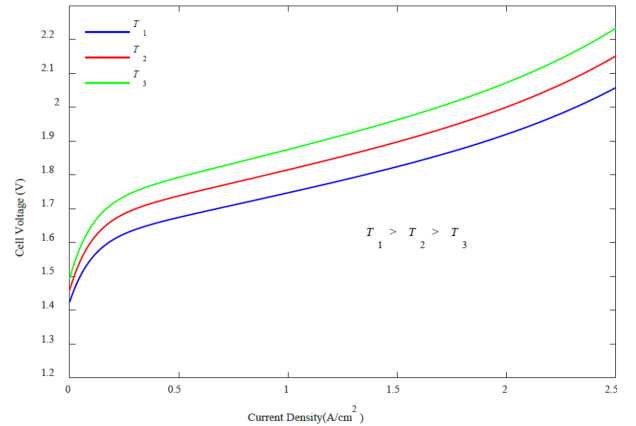

Fig. 2. Polarization curve for different cell temperatures [8]

6) Thermoneutral voltage: The cell voltage with a thermal efficiency of 100%, where neither heating nor cooling is needed, is called thermoneutral voltage. It is 1.48 V in standard conditions, but temperature-dependent, so the polynomial approximation shown in Eq. 12 is made to calculate the

thermoneutral voltage for the actual temperature.

$$V_{th} = 1.5306 - 1.7194 \cdot 10^{-4} \cdot T_{st}$$
$$+ 1.3862 \cdot 10^{-8} \cdot T_{st}^2 + 0.1736 \cdot T_{st}^{-1} \qquad (12)$$

7) Dynamic modeling: While the sum of the overvoltages represents the steady state of the system, setpoint changes and current ripples might influence the output dynamically. This is due to parasitic capacitances that are mainly present in the membrane and the electrodes of the electrolysis cells. A simplified Randles-Warburg equivalent circuit, as shown in Figure 1, allows the consideration of these dynamics in the model. There are two capacitors in the equivalent circuit: one double-layer capacitance C_{dl} accounting for the whole cell, and the electrode capacitance C_d representing load transfer processes in or near the electrodes. The capacitance values for the equivalent circuit can be obtained experimentally by using methods such as the current interruption method or electrochemical impedance spectroscopy. [13]

B. Balance of plant modeling

1) Thermal management: After the stack power consumption itself, the thermal management has the second-largest energy demand in the electrolysis system. PEM electrolyzers can operate in a temperature range of 20 - 100 °C [14], with better efficiencies at higher temperatures (see Figure 2). A thermal managment system is designed to control the stack temperature to a certain reference value within the operating range. It is composed of a heating unit, a cooling unit and a control system, whereas the heating unit is usually only used for startup sequences in cold ambient temperature situations. The electrolyzer would usually be operated at a voltage higher than the thermoneutral voltage, producing excess heat that needs to be discharged from the system. For this reason, only the cooling unit will be considered here, and it is assumed to be a water cooling system with a passive heat sink at ambient temperature. As described in Eq. 13, the required enthalpy flow of cooling water $\dot{Q}_{cl}$ can be calculated by summing up the specific enthalpy flows $\dot{H}$ [15] of the molecules entering and leaving the system and the electrical power P_e provided. To take the thermal dynamics into account, the product of the stack's mass m, the specific heat capacity c_p and the first derivative of the stack temperature T_{st} is added.

$$\dot{Q}_{cl} = \sum \dot{H}_{in} - \sum \dot{H}_{out} + P_e - mc_p \cdot \frac{d}{dt} T_{st} \qquad (13)$$

The stack temperature in this model is set to a reference value of 340 K, and the coolant inlet temperature is assumed to be 300 K. In the scenario of a 120 % overload of the electrolysis stack, the coolant pump needs to deliver 4.8 mol/s (5.2 l/min) of cooling water. The coolant flow is assumed to be proportional to the stack power. For the circulation of the cooling water, an exemplary standard industry pump is considered. The model Danfoss PAHT 2 provides a maximum coolant flow of 5.5 l/min at a rated power of 150 W, assuming a pressure drop among the cooling system of 12 bar. [16]

2) Water supply: The supply of electrolysis stacks with deionized water is crucial for the continuous operation of the system. Taking into account a certain water utilization factor, the water feed-in rate should always match the hydrogen production rate. To prevent cell starvation and failure of the electrolyzer, the ramp-up and ramp-down speed of the water feeding pumps can therefore not be slower than the ramp-up and ramp-down rate of the system itself. The water treatment process, i.e. the production of deionized water from river water, is conducted in the Igiugig water treatment plant and not part of this simulation.

$$\dot{n}_{H_2O} = \frac{1.1 \cdot I}{2F} \cdot \frac{n_{Cells}}{U_{H_2O}} \qquad (14)$$

Eq. 14 shows that the water flow rate is calculated from the stack current I, with an added margin of 10 % to compensate ripples, the Faraday constant F and the number of cells per stack n_{Cells}. To accommodate the imperfect distribution of supply water throughout the electrolysis stack, leading to only a part of the water being used for the reaction, the water utilization factor U_{H_2O} is introduced. In this model, it is set to 0.7. The membrane can then be assumed to be wet at all times, so cell starvation will not occur. The 120 % overload scenario with a stack current of 350 A requires a supply water inflow of 0.32 mol/s (0.35 l/min). Due to these relatively small values, the power consumption of the supply pump can be neglected.

3) Control system: Operating an electrolysis system requires power and current controllers, temperature management and control as well as pump controls for the water feed-in and cooling. However, the energy consumption of these control systems is low compared to the energy consumption of the electrolyzer itself and hence neglected at this point.

C. Hydrogen production modeling

Similar to the water consumption, the hydrogen production rate is also proportional to the stack current I. Due to the capacitive beaviour in non-steady state operation, a part of the stack current does not have an effect on hydrogen production. To take this effect into account and have a more precise hydrogen output model, the current flowing through R_{act} in the equivalent circuit in Fig. 1 is used in Eq. 15.

$$\dot{n}_{H_2} = \frac{I}{2F} \cdot n_{Cells} \qquad (15)$$

D. Heat recovery modeling

Being located in Alaska, Igiugig features temperatures below the freezing point for at least half of a year. Residential space and water heating used to be mainly diesel-fired or electric. To increase the combined efficiency of hydrogen storage plants, the waste heat from the electrolyzer can be recovered, stored in a buffer tank and then be used for space and water heating. The excess heat from the system can be obtained from the energy balance in Eq. 13, the flow temperature is assumed to be 340 K and the return temperature is assumed to be 300 K.

IV. Operation strategies

In the scenario of a fully operative hydrogen storage plant with an electrolyzer, a storage tank and a fuel cell system, the river generator and PV plant as renewable energy sources and the existing battery energy storage system and the diesel generators remaining operative, the Igiugig power grid can be operated in the following way:

The hydrogen storage plant becomes the central component of the energy system, with the Fuel Cell unit being in permanent operation in grid forming mode. The river generator and the PV plant, both being intermittent inverter-based energy sources, feed energy into the grid in grid following mode. The electrolyzer is active to absorb the surplus energy and controlled to a constant setpoint in order to achieve high efficiency. The battery energy storage system captures short-term imbalances in the grid and helps to keep the grid frequency close to its nominal value. The diesel generators serve as backup only, for high grid loads the fuel cell power can be ramped up and the electrolyzer power can be ramped down.

V. Conclusion

This study covers the integration of electrolysis systems as part of hydrogen storage plants into a small electrical island grid. Having a suitable storage solution available facilitates the transformation from fuels imported into the community to energy independence and environment friendly power generation.

As a small but relevant part of this transformation, an electrolysis system with a rated power input of 60 kW has been thoroughly simulated and integrated into a real-time model of the Igiugig power grid from previous works. [9] The model attaches special importance to balance of plant components and heat recovery in an electrolysis system, making it an integral part of the grid of this electrical island. With excess heat of the process being used for space and water heating, competitive efficiencies can be reached, making the installation of a hydrogen based energy storage plant in this grid economically viable.

Further research will investigate the interactions between the components in this island grid, especially in fault scenarios. The presented real-time model allows steady state as well as dynamic simulations and analyses.

References

[1] P. Asmus, "How Alaska Fits into the Global Microgrid Movement," Jul. 2022. [Online]. Available: https://www.uaf.edu/acep-blog/how-alaska-fits-into-the-global-microgrid-movement%20.php

[2] F. University of Alaska, "What is a Microgrid?" 2024. [Online]. Available: https://www.uaf.edu/acep/our-resources/what-is-a-microgrid.php

[3] L. Cohn, "Unlocking the Energy Transition with Solar Added to Microgrids in 8 Remote Alaska Communities," Jul. 2024. [Online]. Available: https://www.microgridknowledge.com/remote-microgrids/article/55092302/unlocking-the-energy-transition-with-solar-added-to-microgrids-in-8-remote-alaska-communities

[4] M. Beaudin, H. Zareipour, A. Schellenberglabe, and W. Rosehart, "Energy storage for mitigating the variability of renewable electricity sources: An updated review," *Energy for Sustainable Development*, vol. 14, no. 4, pp. 302–314, Dec. 2010. [Online]. Available: https://linkinghub.elsevier.com/retrieve/pii/S0973082610000566

[5] L. Kilcher, R. Green, E. Hotchkiss, G. Stark, A. Salmon, and K. Hill, "Igiugig Site Visit Report," National Renewable Energy Laboratory, Golden, CO, USA, Technical Report NREL/TP-5700-79607, 2021. [Online]. Available: https://www.nrel.gov/docs/fy22osti/79607.pdf

[6] A. Salmon, R. Meadows, L. Kilcher, and B. Hirsch, "Igiugig's Journey Toward Sustainability," National Renewable Energy Laboratory, Golden, CO, USA, Technical Report NREL/BR-5700-83816, Dec. 2022. [Online]. Available: https://www.nrel.gov/docs/fy23osti/83816.pdf

[7] I. ORPC, "RivGen® Power System & Integrated Microgrid Solutions." [Online]. Available: https://orpc.co/rivgen-power-system-integrated-microgrid-solutions/

[8] R. Technologies, "RSCAD Power System Manual," 2024.

[9] K. Prabakar, Y. N. Velaga, R. Meadows, B. McGilton, T. Greco, J. Salmon, K. Hill, and L. Tinney, "Understanding Line Losses and Transformer Losses in Rural Isolated Distribution Systems," in *2024 IEEE Rural Electric Power Conference (REPC)*. Tulsa, OK, USA: IEEE, Apr. 2024, pp. 64–69. [Online]. Available: https://ieeexplore.ieee.org/document/10600486/

[10] J. T. Pukrushpan, A. G. Stefanopoulou, and H. Peng, *Control of fuel cell power systems: principles, modeling, analysis, and feedback design*. London: Springer, 2004, oCLC: 55095603.

[11] J. Balej, "Water vapour partial pressures and water activities in potassium and sodium hydroxide solutions over wide concentration and temperature ranges," *International Journal of Hydrogen Energy*, vol. 10, no. 4, pp. 233–43, Jan. 1985.

[12] R. Rodgers and G. Hill, "EQUATIONS FOR VAPOUR PRESSURE VERSUS TEMPERATURE: DERIVATION AND USE OF THE ANTOINE EQUATION ON A HAND-HELD PROGRAMMABLE CALCULATOR," *British Journal of Anaesthesia*, vol. 50, no. 5, pp. 415–424, May 1978. [Online]. Available: https://linkinghub.elsevier.com/retrieve/pii/S0007091217451658

[13] C. Wang, M. Nehrir, and S. Shaw, "Dynamic Models and Model Validation for PEM Fuel Cells Using Electrical Circuits," *IEEE Transactions on Energy Conversion*, vol. 20, no. 2, pp. 442–451, Jun. 2005. [Online]. Available: http://ieeexplore.ieee.org/document/1432859/

[14] M. Carmo, D. L. Fritz, J. Mergel, and D. Stolten, "A comprehensive review on PEM water electrolysis," *International Journal of Hydrogen Energy*, vol. 38, no. 12, pp. 4901–4934, Jan. 2013, num Pages: 34.

[15] B. J. McBride, *Coefficients for Calculating Thermodynamic and Transport Properties of Individual Species*, ser. NASA technical memorandum. Cleveland, OH, USA: NASA Langley Research Center, 1993, no. 4513.

[16] D. A/S, "PAHT pumps Data sheet," 2023.